Published online 18 January 2017

Nucleic Acids Research, 2017, Vol. 45, No. 6 ***3217–3230***
doi: 10.1093/nar/gkw1364

Cdc45-induced loading of human RPA onto single-stranded DNA

Anna Szambowska[1,*], Ingrid Tessmer[2], Piotr Prus[3], Bernhard Schlott[1,4], Helmut Pospiech[1,5] and Frank Grosse[1,6,*]

[1]Research Group Biochemistry, Leibniz Institute on Aging-Fritz Lipmann Institute, Beutenbergstrasse 11, D-07745 Jena, Germany, [2]Rudolf Virchow Center for Experimental Biomedicine, University of Würzburg, Josef Schneider Strasse 2, D-97080 Würzburg, Germany, [3]Biocenter Oulu, P.O. Box 5000, 90014 University of Oulu, Finland, [4]Proteomics Core Facility, Leibniz Institute on Aging-Fritz Lipmann Institute, Beutenbergstrasse 11, D-07745 Jena, Germany, [5]Faculty of Biochemistry and Molecular Medicine, P.O. Box 5000, 90014 University of Oulu, Finland and [6]Center for Molecular Biomedicine, Friedrich-Schiller University, Biochemistry Department, Jena, Germany

Received May 04, 2016; Revised December 22, 2016; Editorial Decision December 27, 2016; Accepted January 02, 2017

ABSTRACT

Cell division cycle protein 45 (Cdc45) is an essential component of the eukaryotic replicative DNA helicase. We found that human Cdc45 forms a complex with the single-stranded DNA (ssDNA) binding protein RPA. Moreover, it actively loads RPA onto nascent ssDNA. Pull-down assays and surface plasmon resonance studies revealed that Cdc45-bound RPA complexed with ssDNA in the 8–10 nucleotide binding mode, but dissociated when RPA covered a 30-mer. Real-time analysis of RPA-ssDNA binding demonstrated that Cdc45 catalytically loaded RPA onto ssDNA. This placement reaction required physical contacts of Cdc45 with the RPA70A subdomain. Our results imply that Cdc45 controlled stabilization of the 8-nt RPA binding mode, the subsequent RPA transition into 30-mer mode and facilitated an ordered binding to ssDNA. We propose that a Cdc45-mediated loading guarantees a seamless deposition of RPA on newly emerging ssDNA at the nascent replication fork.

INTRODUCTION

DNA replication is a fundamental process that duplicates the genetic information of the cell. A major challenge is to deliver complete and only once replicated DNA to each daughter cell. Therefore, the initiation of DNA replication is stringently controlled (1,2). Both, Cdc45 and RPA are essential factors for the initiation and the elongation process (3–7), but a relationship between these proteins has not yet been described. Following the action of S-phase kinases (CDK and DDK) (8), Cdc45 and the four subunits of the GINS complex are integrated into the Mcm2–7 helicase resulting in the 'CMG complex' representing the active replicative DNA helicase in eukaryotes (9). This fully reconstituted helicase unwinds the *origins* of replication and coordinates the assembly of key proteins of the replication machinery, including the DNA polymerase loading factors Ctf4/And-1, MCM10, and the polymerases α and ϵ (10–12). Recent findings demonstrate that Cdc45 binds single stranded DNA (ssDNA) (13,14) and this activity may be important during replication fork stalling (15). On ssDNA, Cdc45 reveals a 3′-5′ sliding polarity, the same as the movement of the replicative CMG helicase on the leading strand template (14). In addition, Cdc45 preferentially binds to single-strand/double-strand (ss/ds) junctions and possibly initiates strand separation by the Mcm2–7 helicase (14). On the other hand, single-particle electron microscopy studies on the entire CMG complex from *Drosophila* led to the suggestion that DNA binding of Cdc45 serves as a guard against occasional slippage of the leading strand from the CMG core channel (16). After DNA unwinding, the newly generated ssDNA is rapidly covered with RPA (7), followed by the recruitment of DNA polymerase α-primase to synthesize RNA primers that are required for initiation of replication (17,18). During strand elongation, RPA stimulates both DNA polymerases α and δ, and it plays a role in DNA polymerase switching and Okazaki fragment processing (19,20). RPA represents a stable complex of three subunits, i.e. RPA70 (70 kDa), RPA32 (32 kDa) and RPA14 (14 kDa) (19–21). Biochemical and biophysical studies together with the crystal structure of truncated hetero-trimer of RPA bound to ssDNA demonstrated that this factor represents a flexible and modular protein containing six oligosaccharide/oligonucleotide binding (OB)-folds (19,20,22,52). Its ssDNA-binding activity is mostly mediated by four DNA binding domains (DBDs), named

*To whom correspondence should be addressed. Tel: +49 3641 65 6105; Fax: +49 3641 65 62 88; Email: szambowska@fli-leibniz.de
Correspondence may also be addressed to Frank Grosse. Tel: +49 3641 65 6290; Fax: +49 3641 65 62 88; Email: fgrosse@fli-leibniz.de

A to D, that bind ssDNA with decreasing affinity (22,23). RPA70, contains the three DBDs, A–C and possesses intrinsic ssDNA-binding activity (24,25). Studies using scanning transmission electron microscopy demonstrated that RPA binds to longer ssDNA substrates in extended conformation (26). However, structural analysis by both X-ray crystallography and small-angle X-ray scattering unveiled that—against intuition—the 30-mer binding mode goes along with a compact protein structure whereas the 10-mer binding uses an extended conformation of the protein (23,27).The N-terminal part of RPA70 subunit (RPA70N) carries a basic cleft that may bind DNA (via DBD-F), but is mainly implicated in protein-protein interactions (28,29). Binding of RPA to ssDNA occurs sequentially and with a defined 5′-3′ polarity resulting in at least two discrete binding states covering 8–10 and 28–30 nucleotides (nt), respectively (22,30,31). The low affinity binding mode (8–10 nts) has a K_D of 50 nM, contrasted by a 1000-fold higher affinity of RPA for ssDNA in the 30 nt binding mode with a K_D of 50 pM (21,24,31,32). For both RPA-binding modes, the 5′ end of the binding site is occupied by RPA70A subdomain, whereas the 3′ end by RPA70B (for 8–10 nt) /or by RPA32D (for 28–30 nt) (24,25,30,33).The high affinity of RPA for ssDNA and its ability to interact with and to modulate a manifold of other proteins assigns it to crucial roles in nearly all DNA metabolic transactions, such as replication, repair, recombination, telomere maintenance, DNA damage response and checkpoint activation (34–36). RPA is also required for viral DNA replication. The simian virus 40 (SV40) utilizes cellular RPA for origin unwinding (37–41) and for loading of the DNA polymerase α/primase complex (18). After large T antigen (T-ag)-mediated unwinding of the viral DNA, the viral helicase loads RPA to stabilize the newly emerging ssDNA (39). This requires physical interaction between the T-ag origin binding domain (OBD) and the RPA domains A and B (RPA70AB). An analogous recruitment of RPA into papilloma viral origins by the helicase E1 had also been demonstrated (42).

Here, we report a loading mechanism for RPA by Cdc45, a component of the human replicative helicase. Cdc45 significantly stimulated binding of RPA to ssDNA and this process required physical contacts between both proteins. In addition, Cdc45 facilitated an ordered assembly of RPA onto ssDNA. The lengths of RPA-bound ssDNA affected its ability to form a ternary complex with Cdc45. Real-time analysis of the kinetics of the Cdc45-induced RPA loading reaction revealed that Cdc45 actively recruited RPA to ssDNA and this process was not concentration-dependent with respect to Cdc45. Therefore, Cdc45 acted as catalyst. Mapping of the interaction surfaces between Cdc45 and RPA revealed contacts of Cdc45 with the RPA70A subdomain. Our findings provide a mechanistic insight into the ssDNA processing functions of RPA at human replication origins, and likely elsewhere in the manifold of RPA-mediated DNA transactions.

MATERIALS AND METHODS

Reagents and oligonucleotides

Agar, yeast extract and tryptone broth were from Carl Roth KG (Karlsruhe, Germany). T4 polynucleotide kinase (PNK) was obtained from Thermo Scientific (Darmstadt, Germany). All other chemicals were from Sigma-Aldrich (Steinheim, Germany). Oligonucleotides in triple HPLC-purified quality were purchased from Purimex (Grebenstein, Germany). The corresponding sequences are listed in Supplementary Table S1.

Radioactive labeling of single-stranded (ss) DNA substrates

5′-ends were labeled with PNK and ^{33}PγATP (5000 Ci/mmol) from Hartmann Analytic (Braunschweig, Germany) for 1 h at 37°C in forward reaction buffer (80 mM Tris–HCl pH 7.4, 10 mM $MgCl_2$, and 5 mM DTT). Reaction was stopped by heating to 72°C for 10 min. Unincorporated nucleotides were removed using Ilustra MicroSpin G-25 columns (GE Healthcare; Freiburg, Germany).

Electrophoretic mobility shift assays (EMSAs)

Reactions (10 μl) contained 4 nM 5′-end labeled DNA and were prepared in 20 mM HEPES–KOH pH 7.5, 1 mM DTT, 100 mM KCl, 7 mM $MgCl_2$ and 40 μg/ml bovine serum albumin (BSA). The indicated amounts of RPA and Cdc45 were added, incubated for 10 min at 30°C and rapidly cooled on ice. Then, 5 μl loading buffer (0.1% bromophenol blue, 0.1% xylene cyanol and 40% glycerol) was added. The samples were separated on 10% native polyacrylamide gels in 89 mM Tris base, 89 mM boric acid and 2 mM EDTA (1× TBE) buffer. After electrophoresis, gels were dried for 1 h at 80°C, exposed to a phosphorimaging screen and visualized with a Phosphor-Imager (Typhoon Trio, GE Healthcare).

Gel shifts experiments with fluorescent labelled ssDNA (FAM-M2) were performed especially as above, using 50nM ssDNA substrate. After electrophoresis the gels were visualized with a Fluorescent-Imager (Typhoon Trio).

Site directed mutagenesis (SDM)

Deletion mutants of human Cdc45 lacking the residues: 154–164 and 137–188 were prepared via site-directed mutagenesis, using plasmid pRSFDuet-1-Cdc45 (14) as a template. Cdc45 Δ154–164 mutant lacking 11 aa from a C-terminal part of disordered region of human Cdc45, whereas Cdc45 (Δ137–188) lacking the whole disordered region and the adjacent alpha helix 6. The following pairs of overlapping primers (Supplementary Table S1) were used to amplify subsequent DNA fragments: Cdc45 Δ154–164 (Cdc45 11 mis up and Cdc45 dis down) and Cdc45 Δ137–188 (Cdc45 dis up and Cdc45 dis and helix down). After amplification, purified PCR products were ligated, and then digested with DpnI enzyme to remove the template DNA. Finally, re-circularized DNA's were transformed into *Escherichia coli* DH5α strain. Deletions were verified via sequencing.

Protein purification

Recombinant human Cdc45 (wild type and deletion mutants) were expressed in bacterial cells and purified as described (14). Heterotrimeric human RPA was overproduced from the plasmid p11d-tRPA, kindly provided by Dr Marc

Wold (University of Iowa). RPA purification was performed as described (53). His-tagged RPA70AB protein was overproduced from the plasmid pSV281, generously provided by Dr Walter Chazin (Vanderbilt University), and purified as described (54). Protein concentration was determined using an assay kit (BioRad). *Escherichia coli* SSB was purchased from Sigma-Aldrich.

Tryptophan fluorescence spectroscopy

Fluorescence was recorded by a Jasco Spectrofluorometer FP 6500 (Jasco Corporation) using Spectra software. Purified recombinant hCdc45 protein (wt or mutants), (30 μg) in the following buffer: 40 mM HEPES–KOH pH 7.5; 200 mM KCl; 1 mM $MgCl_2$; 1 mM DTT and 20% glycerol; was centrifuged at 10 000 rpm for 40 min before the measurements. All experiments were carried out in a 1 × 1 cm quartz cuvette and the excitation was measured at 295 nm. Tryptophan fluorescence was measured in the presence of increasing concentration of GnHCl (8 M). After each addition of GnHCl, solution was mixed, incubated 10 min at room temperature and then continued the measurement. Titration was performed several times to monitor the denaturation profile of the protein.

Atomic force microscopy

For AFM imaging, the DNA contained a 48 nt long ssDNA gap at 30% of the total length of 916 bp DNA fragment (Supplementary Figure S4A) and was produced as described (55). Prior to incubation, the DNA was preincubated at 65°C for 10 min and slowly cooled down to RT to remove potential salt crystals. For experiments, 30 nM RPA, 750 nM Cdc45 or 30 nM RPA + 750 nM Cdc45 were incubated with 90 nM DNA in 20 mM Tris–HCl pH 7.5, 150 mM NaCl, 10 mM DTT, 10 mM $CaCl_2$ for 10 min at room temperature (RT). To verify the presence of multiple RPA molecules on the ssDNA stretches for RPA+Cdc45, we carried out additional experiments with anti-RPA70 antibody (monoclonal, Epitomics, Burlingame, CA, USA). Samples of RPA alone, Cdc45 alone or RPA+Cdc45 and DNA substrate were incubated at concentrations and conditions as above in the presence of 30 nM anti-RPA70 antibody. After incubations, samples were diluted in AFM deposition buffer (20 mM HEPES pH 7.5, 25 mM sodium acetate, 10 mM magnesium acetate). Incubations without antibody were diluted 50-fold, incubations including anti-RPA70 antibody were diluted 100-fold due to higher total protein concentrations. 20 μl of these dilutions were immediately deposited onto freshly cleaved mica, rinsed with ultrapure deionized water and dried in a stream of N_2. AFM scans were performed in air on a Molecular Force Probe (nMFP) 3D BIO atomic force microscope (Asylum Research, Wiesbaden, Germany) in oscillating mode using Olympus OMCL AC240 silicon probes with spring constants of ∼2 N/m and resonance frequencies of ∼70 kHz. Images were captured at scan speeds of 2.5 μm/s and at scan sizes of 1 × 1, 2 × 2 or 4 × 4 μm^2 with corresponding pixel resolutions of 512 × 512, 1024 × 1024 and 2048 × 2048, respectively. For analysis, AFM images were plane-fitted and flattened to third order using the Igor Pro based MFP software. DNA fragment lengths and binding positions of protein molecules on the DNA were measured using ImageJ, as previously described (55). Only DNA fragments with lengths close to the correct, theoretical length of 916 bp (∼311 nm) or within one standard deviation (SD) as obtained from Gaussian fits to the distributions of measured DNA lengths were evaluated. Protein binding positions on the gapped DNA substrate were measured as the distance of peaks from the closer DNA fragment end. The total number of peaks on DNA available for analyses from three independent experiments per protein condition were $n_{RPA} = 654$, $n_{Cdc45} = 532$, $n_{RPA+Cdc45} = 994$ for RPA only, Cdc45 only and RPA+Cdc45, for a total of 783, 461 and 839 DNA molecules that contained peaks, respectively. The resulting position distributions were plotted to reveal the average binding position as the center of a Gaussian fit to the histograms (±1 SD), using the software Origin (OriginLab; Northampton, MA, USA). Only protein peaks bound at the position of the ssDNA gap (at 30% of the DNA length) were taken into further analysis (as indicated in Figure 3B). The employed DNA substrate did not contain any DNA end labels to distinguish between 30% distance from the two different ends. Hence, the binding position distributions are plotted from 0% (DNA fragment end) to 50% (center of DNA fragment) and at the ssDNA gap position (30% of DNA length) they contain a low background of nonspecific binding at 30% from the opposite DNA fragment end. Volumes of protein peaks on the ssDNA gap regions were measured using ImageSXM (S. Barret) software. These volumes can be translated into protein molecular weights (56), using a predetermined standard linear relationship ($V = 1.2 \times (MW) - 5.9$) (57), where V is the AFM volume and MW is protein molecular weight. Volumes were measured for $n_{RPA} = 126$, $n_{Cdc45} = 86$, $n_{RPA+Cdc45} = 97$ peaks bound specifically within the ssDNA gap region on the DNA. For experiments including RPA antibody, $n_{RPA} = 100$, $n_{Cdc45} = 27$, $n_{RPA+Cdc45} = 83$ volumes of peaks bound specifically within the gap region were measured on a total of 326, 122 and 511 DNA molecules containing peaks for RPA only, Cdc45 only and RPA+Cdc45 in two (for Cdc45 only) and three (for RPA only and RPA+Cdc45) independent experiments. Using Origin, distinct states were obtained as the centers of Gaussian fits (±1 SD) to the molecular weight distributions (Figure 3C and E for experiments without and with RPA antibody). For comparison of DNA bound complexes for incubations of RPA alone, Cdc45 alone and RPA together with Cdc45, the measured MWs were analyzed separately for the different protein conditions and their cumulative relative abundances were plotted. Volumes of peaks on the gapped DNA region in the absence of protein were also measured as a negative control (DNA only). Such peaks likely arise from salt microcrystals or due to DNA superstructure formation within the ssDNA regions and can be expected to be present also as a background in samples containing protein. Significances of differences in the cumulative abundances of MWs (Figure 3D) were calculated using the Mann–Whitney U-test implemented in the SPSS software (IBM, Ehningen, Germany).

Real-time analysis of Cdc45–RPA interactions by surface plasmon resonance (SPR)

The affinity between Cdc45 and RPA was measured with a BIAcore 3000 biosensor (GE Healthcare) at 25°C. First, the His_6-tagged Cdc45 protein was immobilized on the surface of the CM5 chip to yield an optical signal of ∼1200 resonance units (RU) using the His-capture kit from GE Healthcare. Remaining active groups were blocked by injecting 1 M ethanolamine (pH 8.5) for 7 min. Binding was analyzed by 5 min injections of different concentrations (8–500 nM) of RPA in HBS buffer (20 mM HEPES–KOH pH 7.5, 150 mM KCl, 1 mM DTT, 3 mM EDTA and surfactant P20). The HBS buffer was injected and the dissociation phase was recorded. The analyses were performed at a flow rate of 30 μl/min. As a control for nonspecific interactions, an empty reference cell was used. Data were evaluated using the Biacore 3000 evaluation software v1.0. Refractive index errors due to bulk effects were corrected using a reference flow cell and subtracting values of blank injections. Dissociation constants were calculated from the kinetic rate constants for Cdc45/RPA complex formation and dissociation and assuming a 1:1 interaction model, as well as from concentration-dependent steady-state binding studies.

Analysis of Cdc45-mediated RPA loading onto ssDNA using SPR

Real-time RPA loading on various lengths of ssDNA in the presence of Cdc45 were measured at 25°C using BIAcore T200. 5′-biotinylated ssDNA [M10 (10 nt) and M2 (34 nt)] were diluted in TNE buffer (10 mM Tris–HCl pH 7.6, 300 mM NaCl and 1 mM EDTA) and immobilized on a streptavidin (SA) coated sensor chip, following the manufacturer's instructions. Experiments were carried out in HBS buffer. RPA titrations (8–1000 nM) were performed with 32 nM Cdc45. Then, Cdc45 titrations (8–1000 nM) were carried out with 32 nM RPA. After each binding event, the HBS buffer was injected over the chip surface and the dissociation phase was recorded. The analyses were performed at 30 μl/min flow rate. Data were evaluated using Biacore 3000 evaluation software v1.0. The results are presented as sensorgrams, obtained after subtraction of the background response signal and correction of the buffer effect. As a control of nonspecific interactions, an empty reference cell was used.

Time–resolved proteolysis by trypsin

Limited proteolysis of His-tagged RPA70AB in the presence of Cdc45 and a 10-mer oligonucleotide (LB-8N) was performed with trypsin (Promega) in 30 mM HEPES–KOH pH 7.5, 100 mM KCl, 1 mM DTT, 7mM $MgCl_2$ at 25°C. Briefly, 15 μM of the protein (100 μl total) (either RPA70AB alone or binary complexes (RPA70AB/10-mer or RPA70AB/Cdc45) or ternary complexes (RPA70AB/10-mer/Cdc45) were pre-incubated for 5 min at 25°C before 5 μl of 0.0125 mg/ml trypsin was added. At the given time points, 20 μl of the reaction mixture was withdrawn and proteolysis was stopped by the addition of 1 μl of 100 mM phenylmethanesulfonyl fluoride (PMSF) and 5 μl of 4× SDS sample buffer. The reaction products were analyzed by SDS-PAGE, followed by Coomassie staining.

Antibodies

The indicated proteins were analysed using rabbit polyclonal antibody anti-Cdc45 H-300 (Santa Cruz Biotechnology; Heidelberg, Germany) or rabbit polyclonal antibody anti-Cdc45 (Merck-Millipore; Darmstadt, Germany), the rabbit monoclonal antibody anti-RPA70 (Epitomics), mouse monoclonal anti-RPA 70, clone B-6 (Santa Cruz Biotechnology); hybridoma supernatant mouse monoclonal anti-RPA32 antibody (58), anti-rabbit IgG, anti-mouse IgG conjugated with horse radish peroxidase (Promega; Mannheim, Germany).

Cdc45-RPA pull-down assay

Cdc45, absorbed to protein A agarose (GE Healthcare) immobilized antibody H-300, was incubated with RPA for 1 h at 4°C. After three washes with 30 mM HEPES–KOH, pH 7.9, 50 mM KCl, 7 mM $MgCl_2$, 0.05% NP-40 and protease inhibitor (Roche, Mannheim), the beads were resuspended in SDS sample buffer and analysed by SDS-PAGE, followed by western blotting with anti-RPA70, anti-RPA32 and anti-Cdc45 antibodies.

Pull-down assay with oligonucleotide titrations

Oligonucleotide titrations were performed with 1-, 10- and 25-fold molar excesses of LB-8N (10-mer) or M2 (34-mer) (Supplementary Table S1), respectively. The ssDNA was added to the washed Cdc45/RPA complexes and incubated for 1 h at 4°C under gentle rotation. After the elution step, bound RPA was detected by SDS-PAGE, followed by western blotting with the anti-RPA32 antibody.

Proteomic mapping of interaction domains (trypsin protection assay)

To identify the contact regions between Cdc45 and RPA we utilized trypsin protection assay combined with mass spectrometry. All reactions and subsequent trypsin digestion was performed in the following buffer: 30 mM HEPES–KOH pH 7.5, 150 mM KCl, 7 mM $MgCl_2$, 1 mM DTT. After complex formation (10 min at 30°C), samples (either singular proteins/or binary/or ternary complexes (equal molar ratio, 15 pmol) were directly subjected to trypsin (Promega) cleavage at a target protein to enzyme ratio of 50:1 (w/w). The processed samples were analyzed with a LC–ESI-MS equipment consisting of an Ettan MDLC™-HPLC (GE Healthcare, Munich, Germany) and a LTQ™ mass spectrometer (Thermo Scientific, Waltham, MA, USA). For protein identification the Thermo Proteome Discoverer 1.0™ software (Thermo Scientific) and a human. fasta protein database (where we included the protein sequences of the native and recombinant RPA and Cdc45, respectively) were used.

Peptide array

For epitope mapping, 185 peptides of human Cdc45 corresponding to the primary sequences of the protein were directly synthesized on a cellulose membrane (Kinexus Bioinformatics Corp., Canada). Each peptide was 15 amino acids long, shift by 3 aa, therefore overlapped 12 amino acids of the previous peptide. The membrane was developed according to the manufacturer's instructions, using firstly negative controls (incubation of the membrane with either: primary and secondary antibodies, or only secondary Ab's or bait protein and secondary Ab's) or probed with bait protein (purified RPA) at the concentration of 1 ug/ml in the blocking buffer (4% skim milk, 5% sucrose in TBS-T). The detection of the protein-bound peptides (spots) was carried out by immunodetection (spots on the membrane were visualized by chemiluminescence using ECL substrate (Pierce). Relative intensities of the spots were quantified by densitometry using Image Quant software. Results were verified using two different primary antibodies.

Model building

Structural models of RPA and Cdc45 with identified tryptic peptides were built using Pymol sessions (63). For RPA modeling, the PDB: 4GNX model was used as a template (23), and for human Cdc45—PDB: 5DGO (62). For preparation of CMG complex model structure PDB: 3JC7 (60) was used and human Cdc45 modeled in place of the yeast homolog.

RESULTS

Physical interactions of human Cdc45 with RPA

An evolutionary predecessor of eukaryotic Cdc45 is the bacterial RecJ nuclease (43,44). In contrast to RecJ, Cdc45 does not harbor an OB-fold that permits strong binding to ssDNA (45). We reasoned that a stronger DNA binding of Cdc45 might be mediated by RPA, a ssDNA binding protein containing six OB-folds. Therefore, we assessed potential interactions between Cdc45 and RPA by performing pull-down assays. These unveiled an association between immobilized Cdc45 and RPA, both RPA70 and RPA32 were detected under this condition (Figure 1A). Surface plasmon resonance (SPR) measurements were employed to quantify binding of Cdc45 to RPA. Recombinant His_6-Cdc45 was immobilized via an anti-His antibody on the surface of a BIAcore chip, and RPA was used as analyte. From the concentration-dependent steady state binding of RPA to Cdc45, a dissociation constant of 115 nM was measured (Figure 1B, Supplementary Figure S2A).

Cdc45 stimulates binding of RPA to ssDNA

To assess potential physiological implications of the observed interaction, we analyzed RPA binding to ssDNA of various lengths in the presence and absence of Cdc45. Gel shift experiments demonstrated an intensification of the RPA-ssDNA band (Figure 2A, C1 (complex I)) as well as the appearance of novel more slowly migrating species, when Cdc45 was present (Figure 2A, C2 (complex II)),

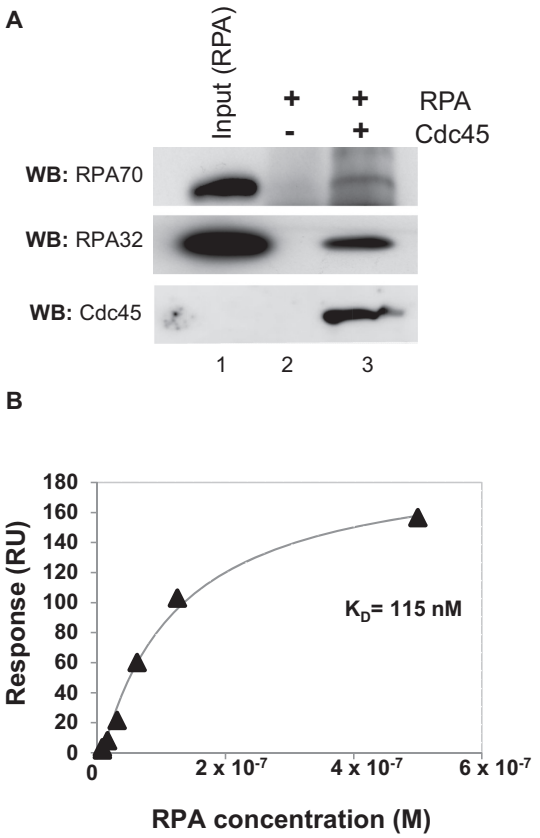

Figure 1. Physical interaction between Cdc45 and RPA. (**A**) Cdc45 pull-down assays. Purified hetero-trimer of RPA (0.46μM) was incubated in the presence (+) or absence (–) of recombinant Cdc45 (0.46 μM), immobilized to protein A beads (GE Healthcare) via the H-300 antibody (Santa Cruz Biotechnology); total volume (250μl). After the washing steps, proteins bound to beads were resolved on a 12% SDS-PAGE gel, followed by western blotting and incubation with antibodies against RPA70, RPA32, and Cdc45. Input (5%). (**B**) Real-time binding analysis of the Cdc45-RPA interaction. The C-terminal His-tagged Cdc45 was immobilized with an anti-His antibody on the surface of the sensor chip (GE Healthcare) and several RPA injections (8; 16; 32; 64; 125 and 500 nM) were recorded. The graph represents a fit of the equilibrium responses for Cdc45 binding of RPA. The dissociation constant was calculated from the concentration-dependent steady-state responses of RPA binding.

whereas no additional band was observed when BSA was added (Figure 2A). This could signify the presence of a ternary complex of Cdc45, RPA and DNA. We therefore performed gel shift experiments with antibodies against RPA70 and Cdc45 (Supplementary Figure S2A). Upon addition of anti-RPA, a supershift of complex C1 was apparent (Supplementary Figure S2A, lanes 4 and 5, C1+Ab). Complex C2 disappeared under these conditions, but no clear supershift of this complex was observed, probably due the lower abundance of C2. In contrast, the mobility of the bound complexes remained unchanged upon addition of antibodies against Cdc45, suggesting that Cdc45 was not part of the band (Supplementary Figure S2A, lane 7). Moreover, under these conditions no binding of Cdc45 to DNA was detectable (Supplementary Figure S2A, lane 8). Furthermore, binding of the *E. coli* single-strand binding protein (SSB) to the 34-mer was not influenced by Cdc45 (Supplementary Figure S3A and B) indicating the absence

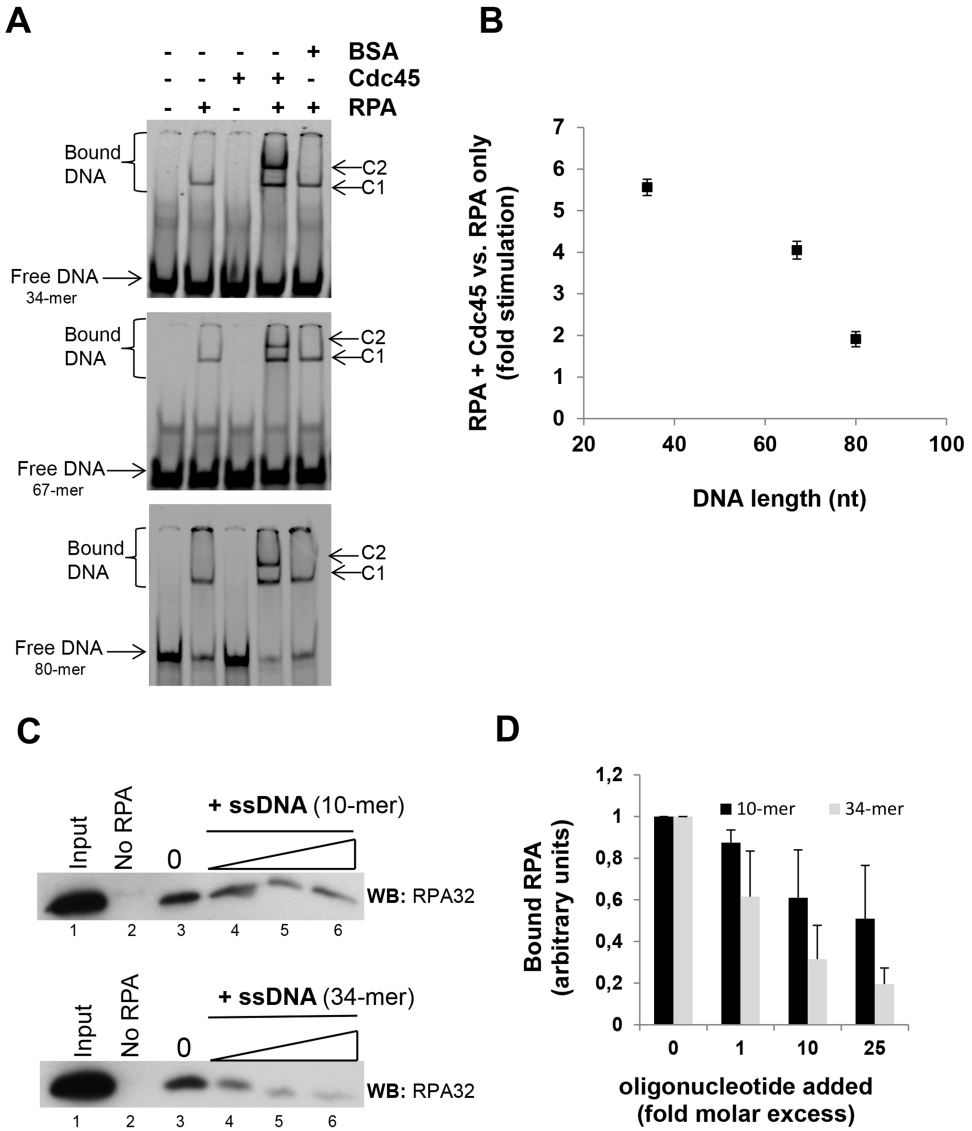

Figure 2. Cdc45-mediated stimulation of RPA binding to various lengths of ssDNA. (**A**) EMSAs were performed with 4 nM 5′-labelled ssDNA (34-mer (M2); 67-mer (M5) and 80-mer (S8), respectively; 10 nM RPA and 200 nM Cdc45. The samples were electrophoresed through 10% non-denaturing polyacrylamide gels. Gels were visualized using a phosphoimager (Typhoon Trio). Free and bound DNA is marked, as well as the complex I (C1) and complex II (C2) respectively. (**B**) The graph represents the amounts of RPA/ssDNA complexes formed in the presence of Cdc45 (for individual lengths of ssDNA), compared to RPA–ssDNA complexes only, as calculated by using the Image-Quant Software. Error bars represent standard deviations obtained from three independent experiments. (**C**) Cdc45–RPA pull-down with oligonucleotide titrations. RPA was incubated with immobilized Cdc45. The pre-formed complexes were challenged with 1-, 10- and 25-fold molar excesses of either a 10-mer or 34-mer ssDNA. The remaining proteins bound to the beads were separated by SDS-PAGE and immunoblotted against anti-RPA32. (**D**) Quantification of the results shown in Figure 2C. The graph represents the relative amounts of RPA-bound complexes, exposed to increasing concentrations of oligonucleotides (10-mer and 34-mer). The amount of bound RPA in complexes, without oligonucleotide was set as one, and the other values were normalized accordingly. Error bars represent standard deviations obtained from three independent experiments.

of concomitant binding of Cdc45 to ssDNA bound by SSB or RPA. Therefore, we concluded that the novel band likely represented a 34-mer ssDNA covered by two molecules of RPA. Next, we studied the stimulatory effect of Cdc45 on ssDNA binding for longer oligonucleotides. Unexpectedly, the stimulatory effect decreased with longer ssDNA substrates. Stimulation was over 5-fold for a 34-mer, about 4-fold for a 65-mer and only 2-fold for an 80-mer (Figure 2B). For further examination, pre-formed RPA-Cdc45 complexes were challenged with ssDNAs. Cdc45-RPA complexes immobilized on beads, were exposed to increasing concentrations of either 10-mer or 34-mer oligonucleotides that correspond to the two major RPA-binding modes (22,31,32). RPA remained stably bound to Cdc45 in the absence of DNA (Figure 2C, lane 3), confirming physical interactions between both proteins as described above. When the Cdc45–RPA complex was exposed to a 10-mer, RPA started to dissociate from the complex. However, titration of bound RPA with a 34-mer, resulted in a much more efficient dissociation of RPA from Cdc45 (Figure 2C, bottom lanes

4–6). This correlated with a much higher affinity of RPA for a long (>30 nt) ssDNA (34). This result strongly suggested that binding of RPA to ssDNA, in particular in the 30-nt binding conformation, competed with its binding to Cdc45, as indicated in Figure 2D. Next, we utilized atomic force microscopy (AFM) to study Cdc45-mediated formation of RPA–ssDNA complexes on a long stretch (48 nt) of ssDNA flanked by double stranded DNA (dsDNA), located at 30% of the DNA fragment length (Supplementary Figure S4A). Analysis of position distributions of the observed complexes on the DNA fragments revealed binding specificity for the ssDNA fragment (Figure 3B). It should be noted that under this condition (high Cdc45 concentration of 750 nM) we also observed binding of Cdc45 in the absence of RPA to the gap (Figure 3A–C), which likely reflects binding of Cdc45 to ss/ds junctions (14). AFM analysis confirmed that addition of Cdc45 to RPA–DNA mixtures resulted in an enhancement of RPA binding to the ssDNA substrate (Figure 3C). Overall numbers of protein peaks per DNA were 0.26, 0.65 and 0.68 for RPA alone, Cdc45 alone and RPA+Cdc45, respectively. Importantly, while the number of protein–DNA complexes was not enhanced for RPA+Cdc45 compared to Cdc45 alone, the overall sizes of the protein–DNA complexes increased significantly (Figure 3C and D). For RPA+Cdc45, increased amounts of DNA-bound complexes with apparent molecular weights of ∼100, 150, 200 and 270 kDa were observed compared to incubations of either RPA or Cdc45 alone (Figure 3C).While the interpretation of the ∼150 kDa species is not quite clear, the MWs of the other three species support Cdc45-mediated increased formation of monomeric, dimeric and most likely trimeric RPA complexes on ssDNA (theoretical MWs of 110, 220 and 330 kDa, respectively). The presence of multiple bound RPA molecules in these complexes was further confirmed by incubations with anti-RPA70 antibody (Figure 3E and Supplementary Figure S4B). The volumes measured for protein–DNA complexes for RPA+Cdc45 incubations in the presence of anti-RPA70 antibody are consistent with dimeric and trimeric RPA complexes onto DNA substrate (apparent MWs of ∼550 and 950 kDa, RPA antibody MW ∼150 kDa).

Increased deposition of RPA on ssDNA by Cdc45

At higher concentrations, RPA forms multiple bound species on ssDNA (22,32) (Supplementary Figure S5A). Moreover, ssDNA-binding of RPA is sequential and displays (at least) two distinct binding modes with covering sizes of 8–10 nt and 25–30 nt, respectively. Upon titration of RPA to a 34-mer with a constant concentration of Cdc45, the amount of the slower migrating distinct protein–DNA complexes increased compared to reactions containing RPA and ssDNA only (Figure 4), in line with our AFM data. Since we have shown that these complexes did not contain Cdc45 (see above), the complexes, designated here as C-1 to C-3, most likely represent a single, two and three molecules of RPA bound to ssDNA, respectively (Figure 4). Apparently, Cdc45 promoted tight binding of RPA onto ssDNA resulting in an increased number of RPA molecules bound per ssDNA.

The kinetics of Cdc45-mediated RPA-loading was measured using SPR. Biotinylated ssDNA (10 and 34nt in size) was immobilized on the surface of a streptavidin (SA) chip. First, RPA titrations to each of the immobilized ssDNA in the presence of a constant concentration of Cdc45 were carried out. As seen by AFM and gel shifts, addition of Cdc45 to ssDNA and RPA resulted in a more efficient RPA binding (green curves), compared to a reaction, in which only RPA and ssDNA were present (blue curve) (Figure 5A). In the second approach, binding of RPA to ssDNA in the presence of increasing amounts of Cdc45 and a constant concentration of RPA was measured (Figure 5B). For these DNA substrates, we observed faster saturation of the binding reaction in the presence of Cdc45 (Figure 5A). Quantification unveiled an about 2-fold increased association rate constant (k_{on}) for Cdc45-mediated RPA binding to a 10-mer and an almost 28-fold increased k_{on} for a 34-mer, strongly suggesting that Cdc45 actively loaded RPA onto ssDNA (Table 1). Moreover, Cdc45 titrations in the presence of constant RPA (32 nM) indicated that RPA loading was not dependent on the Cdc45 concentration in a range of 8–1000 nM, implying that Cdc45 played a catalytic rather than a stoichiometric role (Figure 5B). Cdc45 mainly influenced the k_{on} and barely the dissociation rate constants (k_{off}) on 34-mer (Table 1). For the 10-mer, the dissociation rate constant (k_{off}) was almost 10-fold slower in the presence of Cdc45, indicating a transient stabilization of RPA in the 8–10 nt binding conformation by Cdc45.

Identification of contact regions between Cdc45 and RPA

Trypsin protection assay combined with mass spectrometry was utilized to define the potential binding interface(s) between Cdc45 and RPA on the primary structure level. Pre-formed binary (Cdc45/RPA), and ternary complexes (Cdc45/RPA/10-mer) or singular proteins were subjected to limited trypsin digestion in solution (see Materials and Methods).The resulting tryptic peptides were identified by mass spectrometry (MS). Protection of molecular areas by interactions during Cdc45–RPA complex formation or (via conformational changes within this complex) can render them less accessible or even completely hidden for trypsin cleavage. Additionally, this approach allowed us to capture (and discriminate) tryptic peptides whose generation most likely was only linked to (molecular) changes (probably conformational) upon Cdc45–RPA complex formation or upon binding of protein to ssDNA. Thus, the respective peptides were detected in the complex samples, but not in singular proteins (Supplementary Figure S6A). This was not surprising since RPA alone (23), and probably the Cdc45–RPA complex as well, are highly flexible. Other MS methods can theoretically also provide information about the mutual binding sites (64). We identified four peptides of Cdc45 that might reveal a contact interface with RPA, situated in domain I (Figure 6A, Supplementary Figure S6B), and one peptide placed in the DBD_A subdomain of RPA70 potentially involved in interaction with Cdc45 (Figure 6A, Supplementary Figure S6B). Moreover, using this proteomic approach we were able to discriminate one peptide in DBD_C that most likely underwent conformational changes after binding of RPA to the 10-mer and an-

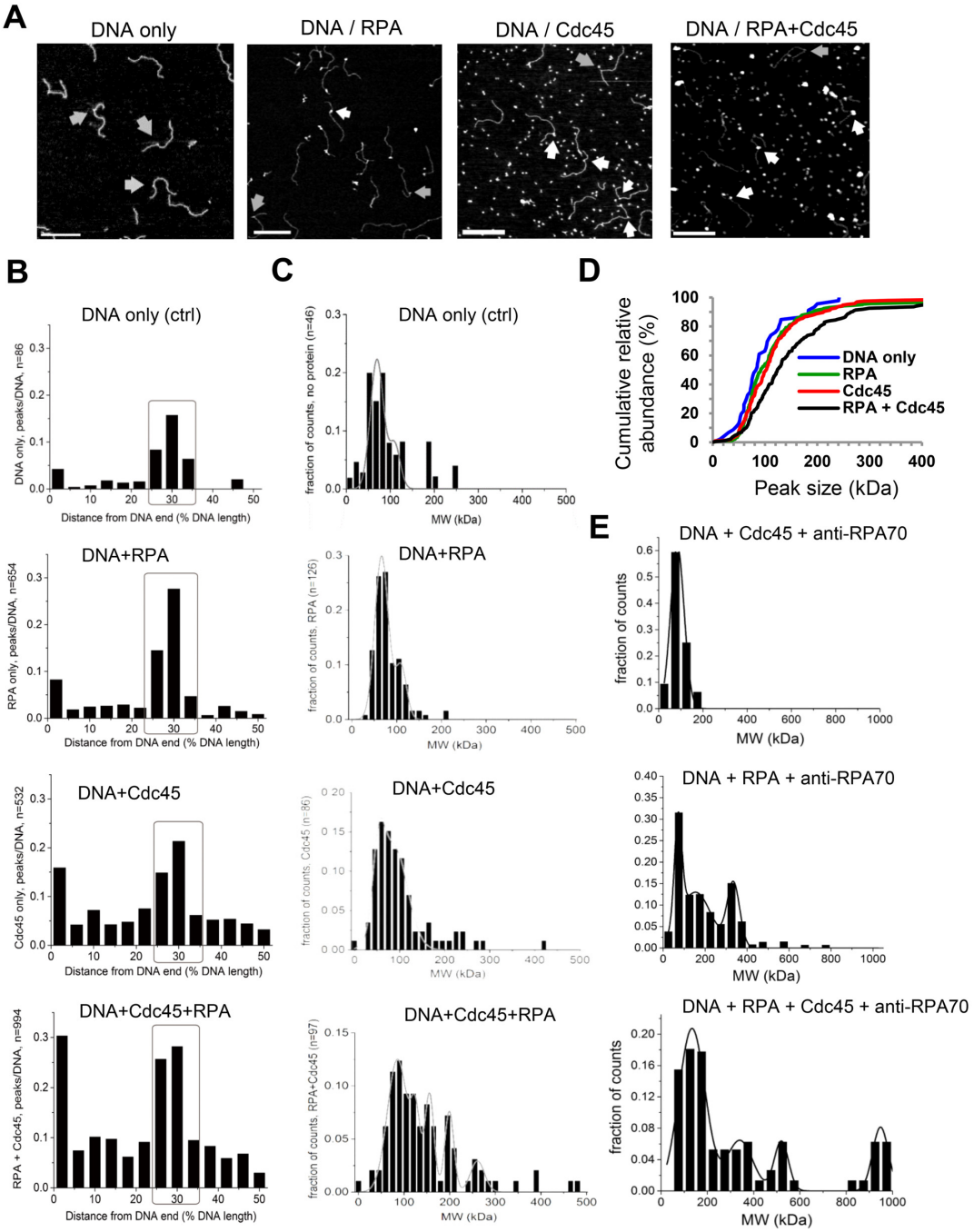

Figure 3. AFM analysis of RPA binding to ssDNA in the presence of Cdc45. (**A**) AFM images of DNA substrate only containing a ssDNA gap at 30% of the DNA length (no protein), RPA only, Cdc45 only, RPA+Cdc45 together in the presence of DNA substrate. The scale bars correspond to 200 nm. White arrows denote the position of potential complexes, grey arrows indicate (smaller) peaks on DNA that likely represent DNA superstructures. (**B**) Position distributions on gapped DNA without protein, DNA+RPA (30nM), DNA+Cdc45 (750nM), and DNA+RPA (30nM)+Cdc45 (750nM). The boxes indicate complexes chosen for analysis. (**C**) Molecular weight distributions obtained from AFM volume analysis of protein–DNA complexes for RPA only (30nM) Cdc45 only (750nM) and RPA + Cdc45 (30 and 750nM, respectively) on ssDNA gap. For comparison, the volumes of the smaller peaks on the ssDNA gapped region in the absence of protein have also been measured (DNA only). Gaussian fits (grey lines) indicate, in addition to the smaller peak volume (∼60 kDa) that we attribute to DNA superstructure, species with apparent molecular weights of ∼110 kDa (monomeric complexes) for RPA only and ∼70 kDa for Cdc45 only. For incubations containing both RPA and Cdc45, a significant enhancement of higher order complexes can be observed (Gaussian fits-grey lines; centering at ∼100, 150, 200 and 270 kDa). Note that the scales of y-axes differ between different plots as a result of different breadths and number of species in the distributions. (**D**) Statistical analyses of peak size distributions from three independent AFM experiments using non-parametric Mann–Whitney U-test implemented in the SPSS software. The following p-values were determined: DNA versus RPA $P = 0.1131$, DNA versus Cdc45 $P = 0.04770$ *, DNA versus RPA+Cdc45 $P = 0.0002719$***, RPA versus Cdc45 $P = 0.4057$, RPA versus RPA+Cdc45 $P = 0.000000896$ *******, Cdc45 versus RPA+Cdc45 $P = 0.0001046$ ***. (**E**) AFM analysis of protein-bound complexes on gapped DNA substrate in the presence of RPA, Cdc45 and anti-RPA70 Ab's (Epitomics, monoclonal). The molecular weights (MW) show a volume increase for complexes bound within the ssDNA gap region (indicating anti-RPA70 antibody binding) for the RPA and RPA+Cdc45 samples but not for Cdc45 alone.

Table 1. Kinetics parameters of Cdc45-mediated RPA loading onto ssDNA

	DNA + RPA*			DNA + RPA + Cdc45**		
ssDNA	K_D (nM)	k_{on} (1/M s)	k_{off} (1/s)	K_D (nM)	k_{on} (1/M s)	k_{off} (1/s)
10-mer	112 ± 14	9.74×10^{-5}	0.0293	44.1 ± 4.7	4.47×10^{-5}	0.0029
34-mer	38 ± 8.1	3.34×10^{-5}	0.0013	1.53 ± 1.3	1.18×10^{-6}	0.0020

Compilation of the data obtained from SPR measurements using the two biotinylated ssDNAs: M10 and M2, purified RPA and Cdc45 proteins. The association rate constant k_{on} is given in (1/M•s), the dissociation rate constant k_{off} in (1/s) and the equilibrium binding constant K_D in (M) for a ssDNA-RPA titration (*) and a ssDNA-RPA titration in the presence of 32 nM Cdc45 (**).

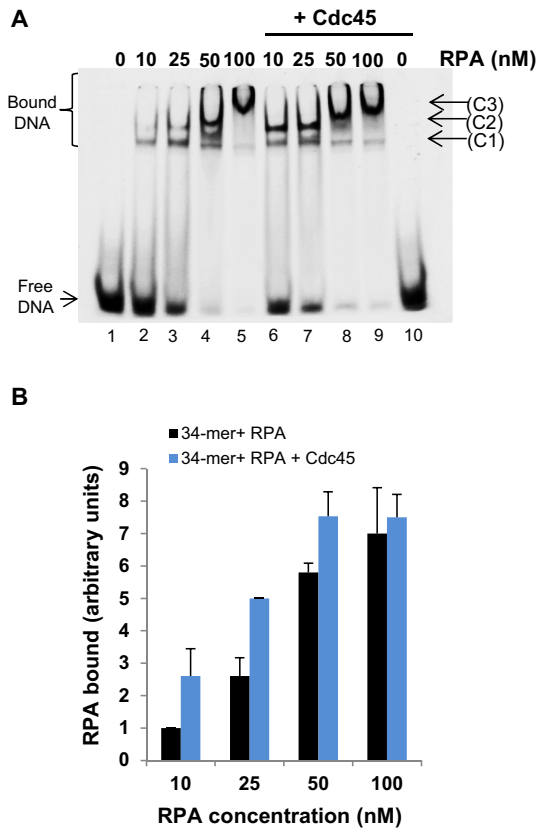

Figure 4. RPA binding to a 34-mer in the presence of Cdc45. (**A**) Gel shift experiments were performed as described for Figure 2 using the 34-mer ssDNA substrate (M2), and the indicated amounts of RPA and 200 nM Cdc45. C1 (complex I), C2 (complex II), C3 (complex III) respectively together with marked free and bound DNA. (**B**) The graph represents the relative amounts of RPA-bound complexes, formed in the presence or absence of Cdc45, analyzed by densitometry and presented as function of the RPA concentration. Amount of complexes observed in the presence of the lowest concentration of RPA without Cdc45 was set to 1 and the other values refer to this value. Error bars represent standard deviations obtained from three independent experiments.

other in DBD_D, (RPA32) that was sensitive to Cdc45–RPA complex formation (Figure 6, Supplementary Figure S6C and D). Using the available structural models of *U. maydis* RPA bound to ssDNA (23) as well as human Cdc45 (62) and the *S. cerevisiae* CMG complex (60), we displayed selected peptides in a constructive manner (Figure 6 and Supplementary Figure S6).The identified peptide of the DBD_A domain (RPA70) (Figure 6B) locates on the opposite side with respect to the ssDNA binding surface consistent with our previous results indicating transient ternary complex formation (Figure 2C). In addition, time-resolved proteolysis studies suggests physical contacts between the RPA70AB subdomain and Cdc45 (Supplementary Figure S7). The RPA70AB linker region was found to be sensitive to proteolysis (44 and Supplementary Figure S7A). Addition of Cdc45 significantly reduced the rate of degradation of the RPA70AB linker (Supplementary Figure S7A), thus implying physical contacts with Cdc45. Similar results were obtained for incubation of RPA70AB with a 10-mer ssDNA (Supplementary Figure S7A). Interestingly, formation of a transient ternary complex between the 10-mer, RPA and Cdc45 provoked a more pronounced protection of the RPA70AB linker against tryptic cleavage (Supplementary Figure S7). For Cdc45, the most prominent contact interface was located at an alpha-helix that protrudes out of the CMG complex and the adjacent disordered region not resolved in the CMG structure (Figure 6C, Supplementary Figure S6D). To elaborate on the identification of interaction sides between Cdc45 and RPA, peptide macroarray experiments were performed. These implicated Cdc45 aa178–189 located at the protruding alpha-helix 6 in contact formation with RPA (Supplementary Figure S8). Based on these results, Cdc45 deletion mutants of the disordered region and alpha helix 6 were constructed and the corresponding proteins purified. Tryptophan fluorescence spectroscopy of both mutants show comparable tryptophan environment and stability against guanidium hydrochloride compared to wt Cdc45 (Supplementary Figure S9). In contrast, both Cdc45Δ154–164aa and Cdc45Δ137–188aa displayed significantly diminished loading of RPA onto ssDNA (Figure 7). Taken together, the region spanning the protruding helix 6 and the adjacent disordered residues of Cdc45 comprise the interaction region for RPA, other peptides of Cdc45, identified originally by trypsin protection assay, located in the middle of the protein and in close proximity to the MCM5 subunit and GINS (Supplementary Figure S6C) most likely were the consequence of conformational changes within Cdc45 upon RPA binding (Supplementary Figure S6).

DISCUSSION

RPA is a central component of eukaryotic DNA metabolism with a major impact on DNA replication. The high affinity of RPA to ssDNA enables protection of exposed ssDNA stretches against nucleases, chemical attacks or binding of inappropriate factors. Interestingly, the ability of many RPA-interacting proteins to facilitate its displacement from ssDNA led to the consideration whether RPA freely diffuses or is actively loaded onto

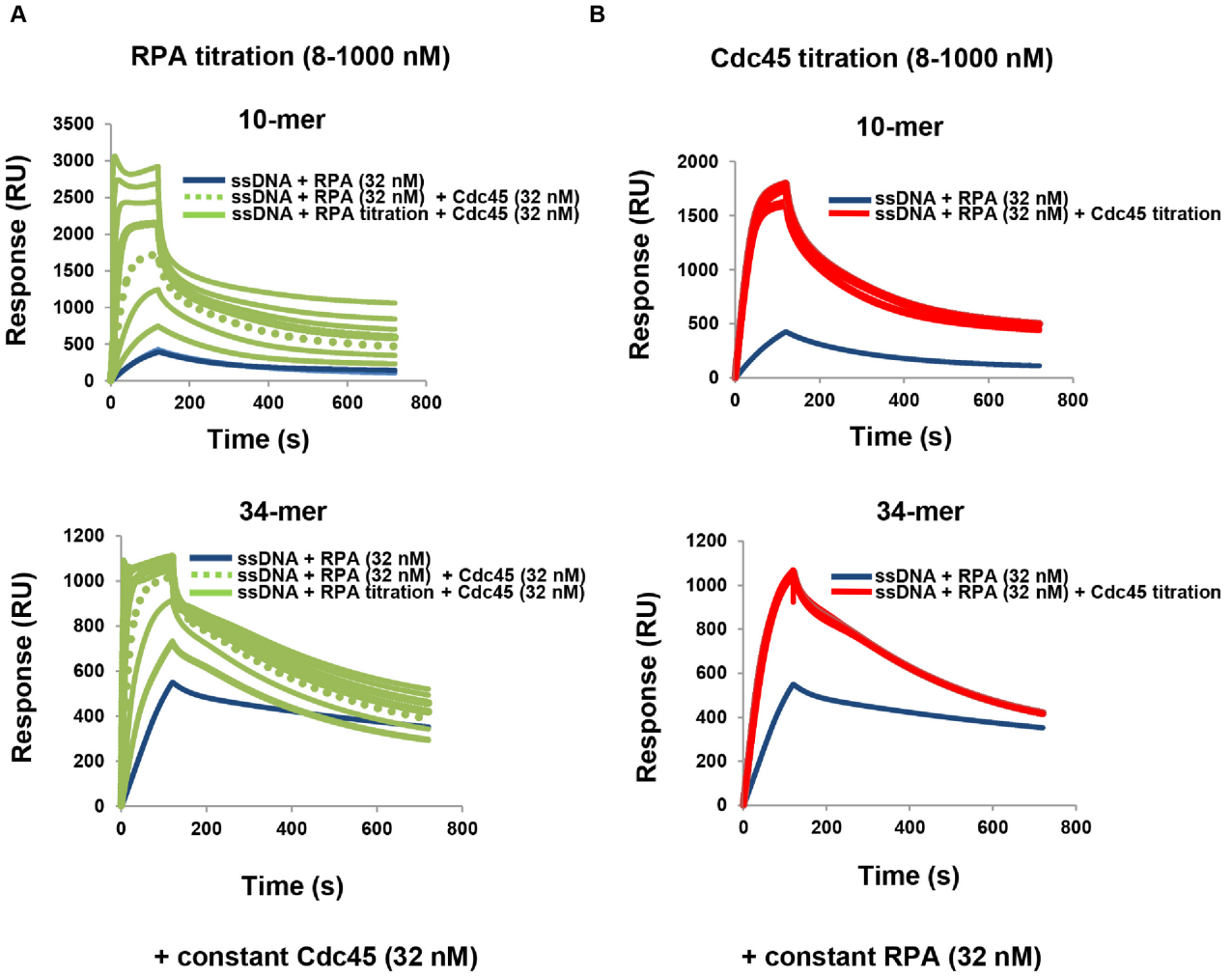

Figure 5. Real-time analysis of Cdc45-mediated RPA loading onto ssDNA. Two biotinylated ssDNA M10 (10-mer) and M2 (34-mer) were immobilized on the surface of a streptavidin (SA) chip (GE Healthcare). (**A**) Sensorgrams of RPA titration (8; 16; 32; 64; 125; 500 and 1000 nM) in the presence of a constant Cdc45 concentration (32 nM). For each individual ssDNA substrate, a graph represents a comparison of the binding of 32 nM RPA to ssDNA (blue curve), with the RPA titration with a constant Cdc45 concentration (green curves). The green dashed curve represents binding of 32 nM RPA to ssDNA in the presence of 32 nM Cdc45. RU (resonance units). (**B**) Sensorgrams of Cdc45 titration (8; 16; 32; 64; 125; 500 and 1000 nM) in the presence of constant (32 nM) RPA. For each individual ssDNA substrate, a graph represents a comparison of the binding of 32 nM RPA to ssDNA (blue curve), with the binding of 32 nM RPA with increasing concentration of Cdc45 (red curves, almost totally superimposed). All measurements were performed using the BIAcore T200 system. Binding was recorded at 25°C at a flow rate of 30 μl/min in 10 mM HEPES–KOH pH 7.5, 1 mM DTT, 1 mM $MgCl_2$, 3 mM EDTA, 150 mM NaCl, and 0.005% surfactant P20. RU (resonance units).

ssDNA (45,46). In this study, we provide strong evidence that Cdc45—an essential component of the eukaryotic replicative DNA helicase—directly loads RPA on the emerging nascent ssDNA. Interestingly, our data indicate that the length of ssDNA bound to RPA regulated the binding stretch between Cdc45 and RPA (Figure 2C and D). We demonstrate formation of a transient ternary complex between RPA, a 10-mer ssDNA, and Cdc45 with a K_D for the Cdc45–RPA interaction in the submicromolar range (Figure 2, Table 1, Figure 1 and Supplementary Figure S6). In contrast, RPA-binding to a 30-mer ssDNA is 1000-fold stronger compared to short ssDNA stretches and lead to dissociation of Cdc45 from the complex (Figure 2C and D). The dissociation of Cdc45 from the ternary complex in the presence of 30-mer is most likely brought about by the conformational change of the RPA quaternary structure from 8–10 nt to 30-nt binding conformation. It is not difficult to imagine that this conformational change completes the RPA loading reaction. To characterize physical contacts between Cdc45 and RPA, we employed several methods (Figures 1–6: Supplementary Figures S6–S9). These studies implicated the DBD_A domain of RPA70 in the interaction with Cdc45 (Figure 6, Supplementary Figure S6). In Cdc45, complex formation with RPA mainly involved sites located in domain I, prominently in a region including part of alpha helix 6 that protrudes out from the CMG complex (Figure 6, Supplementary Figures S6–S9). In addition, using trypsin protection approach we were able to locate peptides in protein areas that most likely take part in conformational changes within both proteins upon complex formation (Figure 6, Supplementary Figure S6). Moreover, our results revealed that the identified DBD_A

A

Peptide	Protein	Remarks
158 **TRLEEEIVEQTMRR** 171	Cdc45	lost upon Cdc45-RPA complex formation
238 **YVTDVGVLQR** 247	Cdc45	lost upon Cdc45-RPA complex formation
311 **LQEFLADMGLPLK** 323	Cdc45	lost upon Cdc45-RPA complex formation
407 **SNLDKLYHGLELAKK** 421	Cdc45	lost upon Cdc45-RPA complex formation
537 **MLHNHFDLSVIELK** 550	Cdc45	appeared upon Cdc45-RPA complex formation
235 **ATAFNEQVDR** 244	RPA70	lost upon Cdc45-RPA complex formation
473 **KENCMYQACPTQDCNKK** 488	RPA70	appeared upon RPA binding to a 10-mer
86 **APTNIVYK** 93	RPA32	appeared upon Cdc45-RPA complex formation

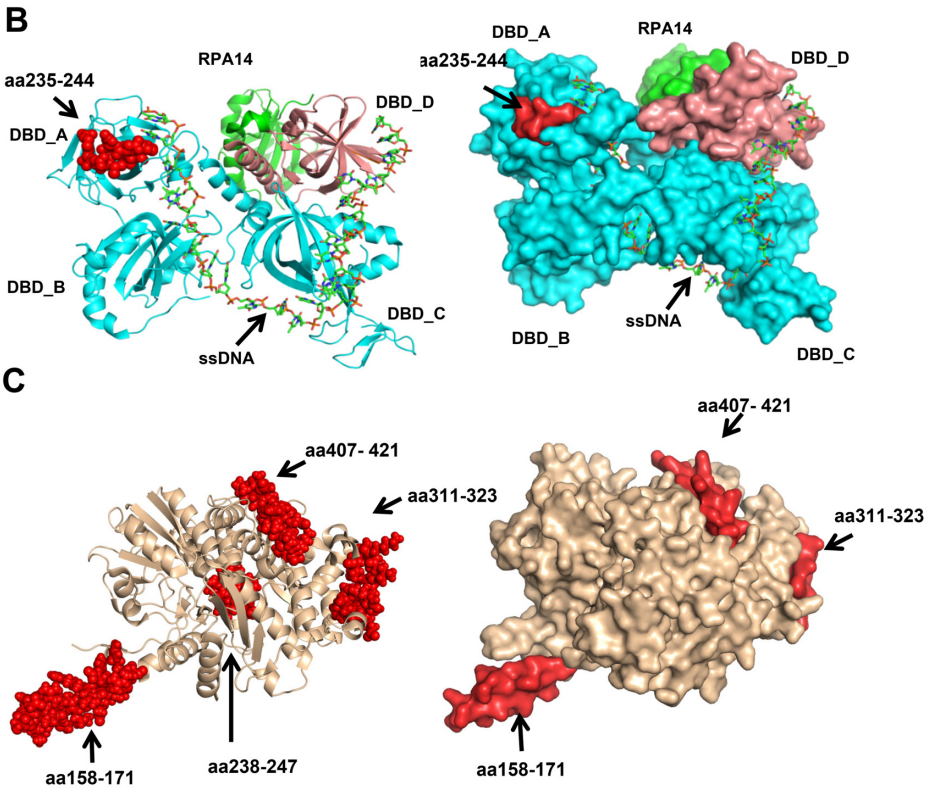

Figure 6. Proteomic approach for identification of 'hotspots' of Cdc45-RPA interaction. (**A**) List of tryptic peptides identified using a proteomic approach. Numbers indicate the position of amino acids. (**B**) Side chain (left) and surface model (right) of *U. maydis* RPA bound to ssDNA (PDB: 4GNX) with RPA70 (DBD_A; DBD_B and DBD_C) marked in light blue; RPA32 (DBD_D) in pink and RPA14 in green. Single-stranded DNA (ssDNA) is marked in orange-green-dark blue. The peptide involved in complex formation displayed as spheres (in red). Arrow denotes the position of the displayed peptide. The amino acids (aa) position of the identified human peptide is given. (**C**) Side chain (left) and surface model (right) of human Cdc45 (PDB: 5DGO) with peptides involved in complex formation with RPA displayed as spheres (in red). Arrows indicate the position of the displayed peptides. The aa position of identified human peptides are given.

binding site in RPA, responsible for contact formation with Cdc45, is located opposite to the ssDNA binding pocket of RPA (23; Figure 6). Thus, Cdc45 and ssDNA do not compete for interaction with RPA, facilitating formation of transient ternary complex and supporting the proposed RPA loading reaction. Quite an opposite scenario was proposed for interaction of RPA70A with Rad51 and XPA, key players in homologous recombination and DNA repair (57). In these cases, a competitive reaction was suggested, where both proteins compete with RPA for its primary ssDNA-binding site, which resulted in displacement of RPA from ssDNA (57). Loading and unloading may also be achieved by different mechanisms. The interaction site described here, located in RPA70A, strongly resembles the contacts between SV40 T-Ag and RPA, which was detected between the origin-binding domain of the viral helicase and RPA70AB (37). Here, direct interaction between human RPA and the simian virus 40 large T-antigen, modulated by the length of ssDNA bound to RPA, is indispensable for *origin* melting and subsequent primer synthesis during SV40 DNA replication (35,36,38). Similarly, the papillomaviral E1 helicase couples DNA unwinding to RPA recruitment on the emerging ssDNA (40). Real-time analyses revealed that Cdc45-mediated RPA loading is catalytic rather than stoichiometric. The surprisingly, high concentrations (≥200 nM) of Cdc45 required for RPA loading in gel shift assays (Figures 2 and 4), are readily explained by the dissociation constant for

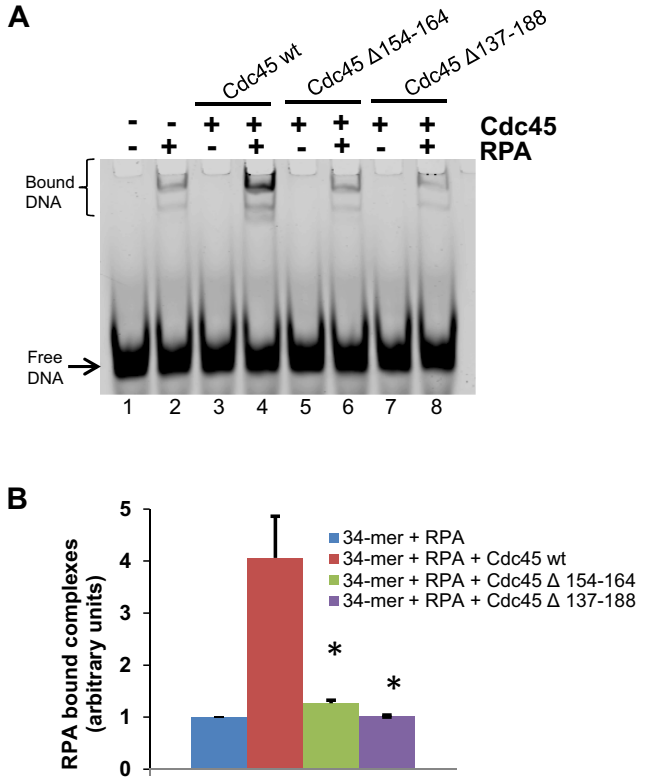

Figure 7. Functional analysis of Cdc45–RPA interaction. (**A**) Gel shift experiments with 50nM fluorescent labeled M2 ssDNA substrate (FAM-M2); RPA (30nM) and Cdc45 wt and mutants (200 nM). After 10 min incubation at 30°C, the mixtures were cooled on ice and 5μl loading dye was added. The samples were resolved by 10% non-denaturing polyacrylamide gel electrophoresis in 1× TBE buffer. Gels were visualized using a fluorescence-imager (Typhoon Trio, GE Healthcare). Free and bound DNA is marked. (**B**) The graph represents relative amounts of RPA-bound complexes, formed in the presence or absence of Cdc45 wt, Cdc45Δ154–164 aa and Cdc45 Δ137–188, analyzed by densitometry. Amount of RPA bound complexes observed without Cdc45 was set to 1 and the other values refer to this value. Error bars represent standard deviations obtained from three independent experiments. Asterics indicate statistically significant changes in RPA binding compared to Cdc45 wt ($P < 0.05$).

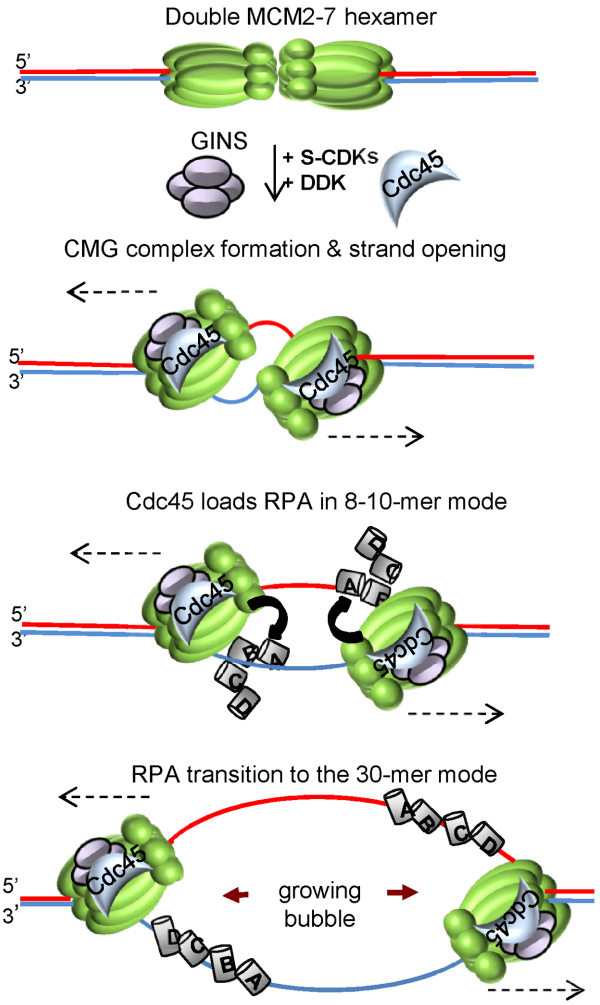

Figure 8. Proposed model for Cdc45-induced loading of RPA onto ssDNA. The Mcm2–7 complex is loaded onto dsDNA. After action of the S-phase kinases (CDK and DDK), Cdc45 and GINS associate with the Mcm2–7 complex to form an active CMG complex. Then, Cdc45 recruits RPA and loads it in the 8–10mer binding mode onto ssDNA. RPA14 is omitted for simplicity. As soon as the ssDNA stretch reaches 25–30 nucleotides, RPA binds to this DNA fragment with high affinity in the 30-mer binding mode. During this transition the physical contacts between hCdc45 and RPA are disrupted.

the Cdc45-RPA complex in the 100 nM range (Figure 1 and 4). Even when both proteins were present at 100 nM each, only half of them would be involved in the DNA encounter complex. Thus, higher concentrations of Cdc45 were necessary to visualize RPA loading by EMSA, but not to catalyze recruitment of RPA onto ssDNA by Cdc45. This was confirmed by SPR measurements showing that the conformational change of RPA did not depend on the concentration of Cdc45 (Figure 5B). Interestingly, a very similar finding was recently reported (47), suggesting that a conformational switch of RPA controls the recruitment of the fork protection proteins TIMELESS and TIPIN, also known as the TIM-TIPIN complex. Different to Cdc45, TIM-TIPIN binds to and stabilizes RPA in the 30-mer binding mode (47). This might contribute to a further consolidation of RPA binding at the opened replication origin and/or for checkpoint activation at stalled replication forks. Because of its apparent binding to the DNA polymerases α, δ and ϵ (48), TIM-TIPIN then may recruit the latter ones to reestablish a halted replication fork.

Based on our findings we propose the following mechanism of Cdc45-catalyzed RPA loading (Figure 8). After CDK/DDK-mediated activation of the eukaryotic CMG helicase, the replication fork is established on each side of the emerging bubble. The here described physical contacts of Cdc45 with RPA70A catalyze the subsequent loading of RPA—in an extended 10-mer binding mode—on the DNA strand. When unwinding by the CMG-complex creates a longer (25–30 nt) ssDNA stretch, transient ternary complex becomes disrupted, because RPA binds with 1000-fold higher affinity to the 30-mer. During this transition a conformational change of RPA disrupts the contact surface between Cdc45 and RPA. It seems most likely that the transient ternary complex is an 'intermediate' substrate that

couples DNA unwinding with RPA loading. Interestingly, Blackwell and Borowiec detected cooperative binding of RPA only in the 8–10 nt binding mode (24). In our model (Figure 8), such a type of cooperativity would allow an ordered placement of RPA on newly emerging DNA without leaving apparent gaps, since we observed ordered deposition of RPA onto ssDNA in the presence of Cdc45 (Figures 3 and 4). On the other hand, a lack of cooperativity of two RPA molecules in the extended conformation should allow an easier removal of RPA, e.g. by intruding DNA polymerases. We assume that the here proposed mechanism might explain the usefulness of the different RPA binding modes in DNA processing pathways. Moreover, it may also explain how the described diffusion-controlled (49,50) RPA-ssDNA interaction still might become stimulated and optimized by enzymes like Cdc45, E1 or T-Ag. Finally, taken the novel function of Cdc45 proposed here in connection with the other roles of Cdc45 described previously (14,15,58,59), one can easily envision how Cdc45 may coordinate strand separation, ssDNA channeling and RPA loading in the context of the replicative CMG helicase.

SUPPLEMENTARY DATA

Supplementary Data are available at NAR Online.

ACKNOWLEDGEMENTS

We are grateful to Prof. Dr Marc Wold (University of Iowa) for providing us the p11-tRPA plasmid overproducing human RPA protein and to Prof. Dr Walter Chazin for the pSV281plasmid that overproduce recombinant RPA70AB protein. The authors thank Dr Kristian Koski (Biocenter Oulu, Finland) for preparation of structural models of RPA and Cdc45, as well as to Anita Willitzer and Christian Massino for excellent technical assistance. The authors are also indebted to Dr H.-K. Gührs for helpful suggestions concerning proteomic approach.

FUNDING

The Fritz Lipmann Institute (FLI) is member of the Science Association 'Gottfried Wilhelm Leibniz' (WGL) and is financially supported by the Federal Government of Germany and the State of Thuringia; Rudolf Virchow Center by the German Research Council (Deutsche Forschungsgemeinschaft, DFG) [FZ 82]. Funding for open access charge: Federal Government of Germany and the State of Thuringia.
Conflict of interest statement. None declared.

REFERENCES

1. Diffley,J.F. (2011) Quality control in the initiation of eukaryotic DNA replication. *Philos. Trans. R Soc. Lond. B Biol. Sci.*, **366**, 3545–3553.
2. Pospiech,H., Grosse,F. and Pisani,F.M. (2010) The initiation step of eukaryotic DNA replication. *Subcell. Biochem.*, **50**, 79–104.
3. Aparicio,T., Ibarra,A. and Mendez,J. (2006) Cdc45-MCM-GINS, a new power player for DNA replication. *Cell Div.*, **1**, 18.
4. Bauerschmidt,C., Pollok,S., Kremmer,E., Nasheuer,H-P. and Grosse,F. (2007) Interactions of human Cdc45 with the Mcm2–7 complex, the GINS complex, and DNA polymerases delta and epsilon during S phase. *Genes Cells*, **12**, 745–758.
5. Hardy,C.F. (1997) Identification of Cdc45p, an essential factor required for DNA replication. *Gene*, **187**, 239–246.
6. Pacek,M., Tutter,A.V., Kubota,Y., Takisawa,H. and Walter,J.C. (2006) Localization of Mcm2–7, Cdc45, and GINS to the site of DNA unwinding during eukaryotic DNA replication. *Mol. Cell*, **21**, 581–587.
7. Zou,L. and Stillman,B. (2000) Assembly of a complex containing Cdc45p, replication protein A, and Mcm2p at replication origins controlled by S-phase cyclin-dependent kinases and Cdc7p-Dbf4p kinase. *Mol. Cell. Biol.*, **20**, 3086–3096.
8. Sclafani,R.A. and Holzen,T.M. (2007) Cell cycle regulation of DNA replication. *Annu. Rev. Genet.*, **41**, 237–280.
9. Ilves,I., Petojevic,T., Pesavento,J.J. and Botchan,M.R. (2010) Activation of the Mcm2–7 helicase by association with Cdc45 and GINS proteins. *Mol. Cell*, **37**, 247–258.
10. Gambus,A., van Deursen,F., Polychronopoulos,D., Foltman,M., Jones,R.C., Edmondson,R.D., Calzada,A. and Labib,K. (2009) A key role for Ctf4 in coupling the Mcm2–7 helicase to DNA polymerase alpha within the eukaryotic replisome. *EMBO J.*, **28**, 2992–3004.
11. Im,J.S., Ki,S.H., Farina,A., Jung,D.S., Hurwitz,J. and Lee,J.K. (2009) Assembly of the Cdc45-Mcm2–7-GINS complex in human cells requires the Ctf4/And-1, RecQL4, and Mcm10 proteins. *Proc. Natl. Acad. Sci. U.S.A.*, **106**, 15628–15632.
12. Kang,Y.H., Galal,W.C., Farina,A., Tappin,I. and Hurwitz,J. (2012) Properties of the human Cdc45/Mcm2–7/GINS helicase complex and its action with DNA polymerase epsilon in rolling circle DNA synthesis. *Proc. Natl. Acad. Sci. U.S.A.*, **109**, 6042–6047.
13. Krastanova,I., Annino,V., Amenitsch,H., Gileadi,O., Pisani,F.M. and Onesti,S. (2012) Structural and functional insights into the DNA replication factor Cdc45 reveal an evolutionary relationship to the DHH family of phosphoesterases. *J. Biol. Chem.*, **287**, 4121–4128.
14. Szambowska,A., Tessmer,I., Kursula,P., Usskilat,C., Prus,P., Pospiech,H. and Grosse,F. (2014) DNA binding properties of human Cdc45 suggest a function as molecular wedge for DNA unwinding. *Nucleic Acids Res.*, **42**, 2308–2319.
15. Bruck,I. and Kaplan,D.L. (2013) Cdc45 protein-single-stranded DNA interaction is important for stalling the helicase during replication stress. *J. Biol. Chem.*, **288**, 7550–7563.
16. Petojevic,T., Pesavento,J.J., Costa,A., Liang,J., Wang,Z., Berger,J.M. and Botchan,M.R. (2015) Cdc45 (cell division cycle protein 45) guards the gate of the Eukaryote Replisome helicase stabilizing leading strand engagement. *Proc. Natl. Acad. Sci. U.S.A.*, **112**, E249–E258.
17. Tanaka,T. and Nasmyth,K. (1998) Association of RPA with chromosomal replication origins requires an Mcm protein, and is regulated by Rad53, and cyclin- and Dbf4-dependent kinases. *EMBO J.*, **17**, 5182–5191.
18. Dornreiter,I., Erdile,L.F., Gilbert,I.U., von Winkler,D., Kelly,T.J. and Fanning,E. (1992) Interaction of DNA polymerase-a-primase with cellular replication protein A and SV40 T-antigen. *EMBO J.*, **11**, 769–77619.
19. Prakash,A. and Borgstahl,G.E. (2012) The structure and function of replication protein A in DNA replication. *Subcell. Biochem.*, **62**, 171–196.
20. Wold,M.S. (1997) RPA: A heterotrimeric, single-stranded DNA binding protein required for eukaryotic DNA metabolism. *Annu. Rev. Biochem.*, **66**, 61–91.
21. Iftode,C., Daniely,Y. and Borowiec,J.A. (1999) Replication protein A (RPA): the eukaryot.ic SSB. *Crit. Rev. Biochem. Mol. Biol.*, **34**, 141–180.
22. Bochkareva,E., Korolev,S., Lees-Miller,S.P. and Bochkarev,A. (2002) Structure of the RPA trimerization core and its role in the multistep DNA-binding mechanism of RPA. *EMBO J.*, **21**, 1855–1863.
23. Fan,J. and Pavletich,N.P. (2012) Structure and conformational change of a replication protein A heterotrimer bound to ssDNA. *Genes Dev.*, **26**, 2337–2347.
24. Blackwell,L.J. and Borowiec,J.A. (1994) Human replication protein A binds single-stranded DNA in two distinct complexes. *Mol. Cell. Biol.*, **14**, 3993–4001.
25. Kim,C., Snyder,R.O. and Wold,M.S. (1992) Binding properties of replication protein A from human and yeast cells. *Mol. Cell. Biol.*, **12**, 3050–3059.
26. Blackwell,L.J., Borowiec,J.A. and Mastrangelo,I.A. (1996) Single-stranded-DNA binding alters human replication protein A

structure and facilitates interaction with DNA-dependent protein kinase. *Mol. Cell. Biol.*, **16**, 4798–807.
27. Brosey,C.A., Yan,C., Tsutakawa,S.E., Heller,W.T., Rambo,R.P., Tainer,J.A., Ivanov,I. and Chazin,W.J. (2013) A new structural framework for integrating replication protein A into DNA processing machinery. *Nucleic Acids Res.*, **41**, 2313–2327.
28. Xu,X., Vaithiyalingam,S., Glick,G.G., Mordes,D.A., Chazin,W.J. and Cortez,D.(2008) The basic cleft of RPA70N binds multiple checkpoint proteins, including RAD9, to regulate ATR signaling. *Mol. Cell. Biol.*, **28**, 7345–7353.
29. Ball,H.L., Ehrhardt,M.R., Mordes,D.A., Glick,G.G., Chazin,W.J. and Cortez,D. (2007) Function of a conserved checkpoint recruitment domain in ATRIP proteins. *Mol. Cell. Biol.*, **27**, 3367–3377.
30. Fanning,E., Klimovich,V. and Nager,A.R. (2006) A dynamic model for replication protein A (RPA) function in DNA processing pathways. *Nucleic Acids Res.*, **34**, 4126–4137.
31. Kim,C., Paulus,B.F. and Wold,M.S. (1994) Interactions of human replication protein A with oligonucleotides. *Biochemistry*, **33**, 14197–14206.
32. Arunkumar,A.I., Stauffer,M.E., Bochkareva,E., Bochkarev,A. and Chazin,W.J. (2003) Independent and coordinated functions of replication protein A tandem high affinity single-stranded DNA binding domains. *J. Biol. Chem.*, **278**, 41077–41082.
33. Iftode,C. and Borowiec,J.A. (2000) 5′-3′ molecular polarity of human replication protein A (hRPA)binding to pseudo-origin DNA substrates. *Biochemistry*, **39**, 11970–11981.
34. Oakley,G.G. and Patrick,S.M. (2010) Replication protein A: directing traffic at the intersection of replication and repair. *Front. Biosci.*, **15**, 883–900.
35. Smith,J., Zou,H. and Rothstein,R. (2000) Characterization of genetic interactions with RFA1: the role of RPA in DNA replication and telomere maintenance. *Biochimie*, **82**, 71–78.
36. Bochkareva,E., Kaustov,L., Ayed,A., Yi,G.S., Lu,Y., Pineda-Lucena,A., Liao,J.C., Okorokov,A.L., Milner,J., Arrowsmith,C.H. and Bochkarev,A. (2005) Single-stranded DNA mimicry in the p53 transactivation domain interaction with replication protein A. *Proc. Natl. Acad. Sci. U.S.A.*, **102**, 15412–15417.
37. Dean,F.B., Bullock,P., Murakami,Y., Wobbe,C.R., Weissbach,L. and Hurwitz,J. (1987) Simian virus 40 (SV40) DNA replication: SV40 large T antigen unwinds DNA containing the SV40 orgin of replication. *Proc. Natl. Acad. Sci. U.S.A.*, **84**, 16–20.
38. Dodson,M., Dean,F.B., Bullock,P., Echols,H. and Hurwitz,J (1987) Unwinding of duplex DNA from the SV40 origin of replication by T antigen. *Science*, **238**, 964–967.
39. Jiang,X., Klimovich,V., Arunkumar,A.I., Hysinger,E.B., Wang,Y., Ott,R.D., Guler,G.D., Weiner,B., Chazin,W.J. and Fanning,E. (2006) Structural mechanism of RPA loading on DNA during activation of a simple pre-replication complex. *EMBO J.*, **25**, 5516–5526.
40. Melendy,T. and Stillman,B. (1993) An interaction between replication protein A and SV40 T antigen appears essential for primosome assembly during SV40 DNA replication. *J. Biol. Chem.* **268**, 3389–3395.
41. Wold,M.S., Li,J.J. and Kelly,T.J. (1987) Initiation of simian virus 40 DNA replication in vitro: Large-tumor-antigen- and origin-dependent unwinding of the template. *Proc. Natl. Acad. Sci. U.S.A.*, **84**, 3643–3647.
42. Loo,Y.M. and Melendy,T. (2004) Recruitment of replication protein A by the papillomavirus E1 protein and modulation by single-stranded DNA. *J. Virol.*, **78**, 1605–1615.
43. Lovett,S.T. and Kolodner,R.D. (1989) Identification and purification of a single-stranded-DNA-specific exonuclease encoded by the recJ gene of Escherichia coli. *Proc. Natl. Acad. Sci. U.S.A.*, **86**, 2627–2631.
44. Sanchez-Pulido,L. and Ponting,C.P. (2011) Cdc45: the missing RecJ ortholog in eukaryotes? *Bioinformatics*, **27**, 1885–1888.
45. Sutera,V.A. Jr, Han,E.S., Rajman,L.A. and Lovett,S.T. (1999) Mutational analysis of the RecJ exonuclease of Escherichia coli: identification of phosphoesterase motifs. *J. Bacteriol.*, **181**, 6098–6102.
46. Gomes,X.V., Henricksen,L.A. and Wold,M.S. (1996) Proteolytic mapping of human replication protein A: evidence for multiple structural domains and a conformational change upon interaction with single-stranded DNA. *Biochemistry*, **35**, 5586–5595.
47. Arunkumar,A.I., Klimovich,V., Jiang,X., Ott,R.D., Mizoue,L., Fanning,E. and Chazin,W.J. (2005) Insights into hRPA32 C-terminal domain–mediated assembly of the simian virus 40 replisome. *Nat. Struct. Mol. Biol.*, **12**, 332–339.
48. Vassin,V.M., Wold,M.S. and Borowiec,J.A. (2004) Replication protein A (RPA) phosphorylation prevents RPA association with replication centers. *Mol. Cell. Biol.*, **24**, 1930–1943.
49. Witosch,J., Wolf,E. and Mizuno,N. (2014) Architecture and ssDNA interaction of the Timeless-Tipin-RPA complex. *Nucleic Acids Res.*, **42**, 12912–12927.
50. Cho,W.H., Kang,Y.H., An,Y.Y., Tappin,I., Hurwitz,J. and Lee,J.K. (2013) Human Tim-Tipin complex affects the biochemical properties of the replicative DNA helicase and DNA polymerases. *Proc. Natl. Acad. Sci. U.S.A.*, **110**, 2523–2527.
51. Patrick,S.M., Oakley,G.G., Dixon,K. and Turchi,J.J. (2005) DNA damage induced hyperphosphorylation of replication protein A. 2. Characterization of DNA binding activity, protein interactions, and activity in DNA replication and repair. *Biochemistry*, **44**, 8438–8448.
52. Schubert,F., Zettl,H., Hafner,W., Krauss,G. and Krausch,G. (2003) Comparative thermodynamic analysis of DNA–protein interactions using surface plasmon. *Biochemistry*, **42**, 10288–10294.
53. Henricksen,L.A., Umbricht,C.B. and Wold,M.S.(1994) Recombinant replication protein A: expression, complex formation, and functional characterization. *J. Biol. Chem.*, **269**, 11121–11132. Erratum in: *J. Biol. Chem.*, **10** (23), 16519.
54. Pfuetzner,R.A., Bochkarev,A., Frappier,L. and Edwards,A.M. (1997) Replication Protein A. Characterization and crystallization of the DNA binding domain. *J. Biol. Chem.*, **272**, 430–434.
55. Buechner,C.N. and Tessmer,I. (2013) DNA substrate preparation for atomic force microscopy studies of protein–DNA interactions. *J. Mol. Recognit.*, **26**, 605–617.
56. Ratcliff,G.C. and Erie,D.A. (2001) A novel single-molecule study to determine protein–protein association constants. *J. Am. Chem. Soc.*, **123**, 5632–5635.
57. Roth,H.M., Römer,J., Grundler,V., van Houten,B., Kisker,C and Tessmer,I. (2012) XPB helicase regulates DNA incision by the Thermoplasma acidophilum endonuclease Bax1. *DNA Repair (Amst.)*, **11**, 286–293.
58. Coverley,D., Kenny,M. K., Lane,D. P. and Wood,R. D.(1992) A role for the human single-stranded DNA binding protein HSSB/RPA in an early stage of nucleotide excision repair. *Nucleic Acids Res.*, **20**, 3873–3880.
59. Stauffer,M.E. and Chazin,W.J. (2004) Physical interaction between replication protein A and Rad51 promotes exchange on single-stranded DNA. *J. Biol. Chem.*, **279**, 25638–25645.
60. Yuan,Z., Bai,L., Sun,J., Georgescu,R., Liu,J., O'Donnell,M.E. and Li,H. (2016) Structure of the eukaryotic CMG helicase suggests a pumpjack motion for translocation. *Nat. Struct. Mol. Biol.*, **23**, 217–224.
61. Costa,A, Renault,L, Swuec,P., Petojevic,T., Pesavento,J.J., Ilves,I., MacLellan-Gibson,K., Fleck,R.A., Botchan,M.R. and Berger,J.M. (2014) DNA binding polarity, dimerization, and ATPase ring remodeling in the CMG helicase of the eukaryotic replisome. *Elife*, **3**, e03273.
62. Simon,A.C., Sannino,V, Costanzo,V and Pellegrini,L. (2016) Structure of human Cdc45 and implications for CMG helicase function. *Nat. Commun.*, **7**, 11638.
63. The PyMOL Molecular Graphics System, Version 1.6 Schrödinger, LLC.
64. Tran,B.Q., Goodlett,D.R. and Goo,Y.A. (2016) Advances in protein complexes analysis by chemical cross-linking coupled with mass spectrometry (CXMS) and bioinformatics. *Biochim. Biophys. Acta*, **1864**, 123–129.